HF beam parameters in ELF/VLF wave generation via modulated heating of the ionosphere

M. B. Cohen,[1] M. Golkowski,[2] N. G. Lehtinen,[1] U. S. Inan,[1,3] and M. J. McCarrick[4]

Received 31 January 2012; revised 18 April 2012; accepted 18 April 2012; published 25 May 2012.

[1] ELF/VLF (0.3–30 kHz) wave generation is achievable via modulated HF (3–30 MHz) heating of the lower ionosphere in the presence of natural currents such as the auroral electrojet. Using the 3.6 MW High Frequency Active Auroral Research Program (HAARP) facility near Gakona, AK, we investigate the effect of HF frequency and beam size on the generated ELF/VLF amplitudes, as a function of modulation frequency, and find that generation in the Earth-ionosphere waveguide generally decreases with increasing HF frequency between 2.75–9.50 MHz. HAARP is also capable of spreading the HF power over a wider area, and we find that a larger beam area yields larger generated amplitudes on the ground. Measurements are shown to generally agree with a theoretical model, which is then applied to also predict the effect of HF beam parameters on magnetospheric injection with HAARP.

Citation: Cohen, M. B., M. Golkowski, N. G. Lehtinen, U. S. Inan, and M. J. McCarrick (2012), HF beam parameters in ELF/VLF wave generation via modulated heating of the ionosphere, *J. Geophys. Res.*, *117*, A05327, doi:10.1029/2012JA017585.

1. Introduction

[2] In recent decades, Extremely Low Frequency (ELF, 300–3000 Hz) and Very Low Frequency (VLF, 3–30 kHz) waves have been generated via heating of the lower ionosphere (50–100 km altitude) with High Frequency (HF, 3–10 MHz) radio waves. Because HF heating of the lower ionosphere changes the conductivity, on/off modulation of the HF heating at a desired ELF/VLF frequency imposes that modulation pattern onto the ionospheric currents. In the presence of natural currents such as the auroral or equatorial electrojet, modulated HF heating thus turns the lower ionosphere into a radiating antenna.

[3] Since the first observations by *Getmantsev et al.* [1974], significant research efforts have gone into characterizing the physical processes involved in this indirect method of ELF/VLF wave generation, and into possible means of increasing the generated amplitudes. One notable application of ELF/VLF wave generation is for long distance communications, since these frequencies efficiently reflect at both the Earth and lower ionosphere, and can thus propagate to global distances. ELF/VLF waves are thus also a useful diagnostic tool for the lower ionosphere from which they reflect. Furthermore, controlled injection of ELF/VLF waves into the magnetosphere is an effective method for probing the radiation belts, and for studying the gyroresonant interaction between energetic electrons and whistler mode waves.

[4] Conventional VLF transmitters operating above 10 kHz are typically tuned to transmit near a single frequency using a vertical antenna mast, since the wavelength is substantially longer than a practically realizable antenna, and the ground conductivity nullifies any horizontal current. Below 10 kHz, even this design becomes too inefficient for practical use. Modulated HF heating provides the distinct advantage of being able to operate over a much broader ELF/VLF frequency range, well below 10 kHz, since the natural antenna is tens of km long and far away from the ground.

[5] A number of facilities have been utilized for experimentation in this area. The ionospheric observatory near Arecibo, Puerto Rico [*Ferraro et al.*, 1982], and the observatory at Jicamarca, Peru [*Lunnen et al.*, 1984], were both used to generate weak ELF signals utilizing the equatorial dynamo current. High latitude facilities utilizing the auroral electrojet have thus far had more success at strong ELF generation. The HIPAS facility near Fairbanks, Alaska, utilized a 150 kW transmitter array operating at 2.85 MHz, generating ELF/VLF waves with phase modulation, double-frequency excitation, and amplitude modulation (AM) [*Villaseñor et al.*, 1996], until 2009. The HIPAS facility also utilized an 'array de-phasing' technique, to spread the power over a wider area, aiding in the generation of waves in the Schumann resonance range [*McCarrick et al.*, 1990]. The EISCAT facility near Tromsø, Norway, was utilized for a wide variety of ELF/VLF experiments [*Stubbe et al.*, 1981]. The 1 MW radiated, 200–300 MW effective radiated power (ERP) Tromsø HF heater was

[1]Department of Electrical Engineering, Stanford University, Stanford, California, USA.
[2]Department of Electrical Engineering, University of Colorado Denver, Denver, Colorado, USA.
[3]Department of Electrical Engineering, Koc University, Istanbul, Turkey.
[4]Advanced Technologies, Marsh Creek LLC, Washington, DC, USA.

Corresponding author: M. B. Cohen, Department of Electrical Engineering, Stanford University, 350 Serra Mall Room 356, Stanford, CA 94305, USA. (mcohen@stanford.edu)

0148-0227/12/2012JA017585

Table 1. Radiated Power (and ERP), in Megawatts, of HAARP Beam Modes

f (MHz)	Narrow	Broad-NS	Broad-EW	Broad-Full
2.75	3.24 (417)	2.66 (100)	2.84 (102)	2.27 (25)
3.25	3.35 (575)	3.02 (151)	3.17 (155)	2.81 (40)
4.50	3.13 (1023)	3.02 (269)	3.10 (275)	2.95 (72)
6.80	3.31 (2291)	3.28 (631)	3.31 (631)	3.28 (170)
7.80	3.24 (2884)	3.24 (776)	3.24 (776)	3.20 (214)
9.50	2.88 (3802)	2.88 (1023)	2.88 (1288)	2.88 (275)

typically 100% square wave AM at HF frequencies from 2.75 to 8 MHz. Signals were also detected at distances of 550 km from Tromsø [*Barr et al.*, 1986], and 2200 km [*Barr et al.*, 1991].

[6] More recently, the HAARP near-field phased-array HF facility near Gakona, Alaska (62° 22′ N, 145° 9′ W), has been used to generate ELF/VLF signals that have been observed as far as 4400 km [*Moore et al.*, 2007; *Cohen et al.*, 2010c], as well as injected into the magnetosphere and observed in the geomagnetic conjugate region [*Inan et al.*, 2004; *Gołkowski et al.*, 2008, 2011]. In 2007, an upgrade of HAARP was completed, increasing its capacity from 48 active elements, 960 kW input power, and 175 MW ERP (at 3.25 MHz), to 180 active elements, 3.6 MW input power, and ∼400 MW ERP (at 3.25 MHz). The array de-phasing technique described by *McCarrick et al.* [1990] can also be utilized at HAARP.

[7] The generation of these ELF/VLF waves is strongly affected by the D-region ionospheric electron density and the electrojet strength. These quantities are known to be highly variable and dependent upon geomagnetic conditions. However, the choice of HF heating parameters is also quite important. For instance, proper utilization of motion of the HF beam can yield 7–11 dB more ELF/VLF power in the Earth-ionosphere waveguide [*Cohen et al.*, 2008b, 2010b], and 5–7 dB more power radiated into the magnetosphere [*Cohen et al.*, 2011].

[8] We consider the effect of HF frequency, beam width, and ERP, on generated ELF/VLF amplitudes, both near the heated region, at longer distances in the Earth-ionosphere waveguide, and in the magnetosphere.

2. Description of Experiment

[9] We compare the generated ELF/VLF amplitudes for six different combinations of HF frequencies, and four different beam shapes, for a total of 24 modes. The six HF frequencies are 2.75 MHz, 3.25 MHz, 4.50 MHz, 6.80 MHz, and 9.50 MHz. The four beam shapes are a narrow beam, a beam broadened in each of the N/S and E/W directions, and a beam broadened in both directions. The HAARP grid is oriented ∼14° east of north. In each mode, HAARP transmits at its highest allowable power level. The HAARP HF array is capable of generating other beam shapes (such as a donut-shaped "twisted" beam) but they are not considered here.

[10] Table 1 shows the transmitted HF power (radiated and effective) resulting from each of the modes we consider. The values in each panel are referenced to the power flux at the center of the beam, or $GP/(4\pi r^2)$, where GP (gain times input power) is the ERP, and r is the distance. As the HF frequency increases, the beam becomes more tightly focused, thereby increasing the ERP. The sidelobes also become thinner and more tightly spaced. Broadening the beam effectively merges the main lobe with the adjacent sidelobes, thereby decreasing the ERP while maintaining roughly the same radiated power, and generating an elongated beam. At the lower HF frequencies (especially for a broadened beam) there are significant terminal reflections from the imperfectly matched HF array elements, so that not all of HAARPs 3.6 MW input power is radiated. Figure 1 shows the HF power pattern reaching 60 km altitude from HAARP, over a 100 km side square area, for each of the 24 modes.

[11] For each mode, we generate ELF/VLF waves with 100% square wave amplitude modulation of the HF power. To compare the ELF/VLF generation for each beam mode, a series of two second long constant frequency ELF/VLF tones are transmitted for each mode, from 500 Hz to 7.5 kHz (15 total), with ∼500 Hz spacing. The HAARP beam is pointed vertically. Between each mode, a hardware-imposed 30 second interruption allows re-tuning for the next mode, resulting in 60 s for each cycle. This 60 second cycle repeats once for each of the modes at a given HF frequency (narrow, broad-NS, broad-EW, broad-full). And the four minute cycle for an HF frequency is repeated seven times, for a total of 28 min, in the following order: 3.25 MHz, 2.75 MHz, 4.50 MHz, 6.80 MHz, 7.80 MHz, 9.50 MHz, 3.25 MHz. For at least 60 s before and after the 28-minute sequence begins, the HAARP heater is off.

[12] ELF/VLF data are taken with the 'AWESOME' receiver, described by *Cohen et al.* [2010c]. These consist of two orthogonal air-core loop antennas, sensitive to magnetic fields with amplitudes as low as a few fT/rt-Hz in the ∼0.3–47 kHz band, with GPS synchronization and 16 bit (96 dB) dynamic range. Receivers utilized here are placed in Chistochina (62.62°N, −144.62°W, 37 km from HAARP), and Kodiak (57.87°N, 152.88°W, 661 km from HAARP).

[13] Figure 2 shows a sample spectrogram (window length of 40 ms) taken during one of the experiments. On this particular day (20-Sep-2010), the experiment was run from 2001–2029 UT, and shown are the transmitted sequences for 3.25 MHz narrow beam (2001 UT, upper panel) and the 9.50 MHz narrow beam (2021 UT, lower panel). For each pulse, spaced out by ∼500 Hz, the fundamental frequency is clearly observed at Chistochina, along with a number of higher harmonics which are ignored here. For each received tone, the magnetic field signal at the fundamental frequency is integrated over the entire 2-second length, and the quadrature sum of the two channels yields a magnitude measurement. The lower panel shows results from the weakest ELF of the 24 HF beam configuration modes. The signals are still clearly visible in the spectrogram, and integration at the full 2 s gives all signals above the noise floor. The same procedure can be repeated on empty data from the same period, to determine comparative noise levels. These noise levels can be used to establish error bars based on the SNR of each received tone.

3. Observations

[14] The amplitudes of generated waves received near to HAARP provide useful information, since they are routinely

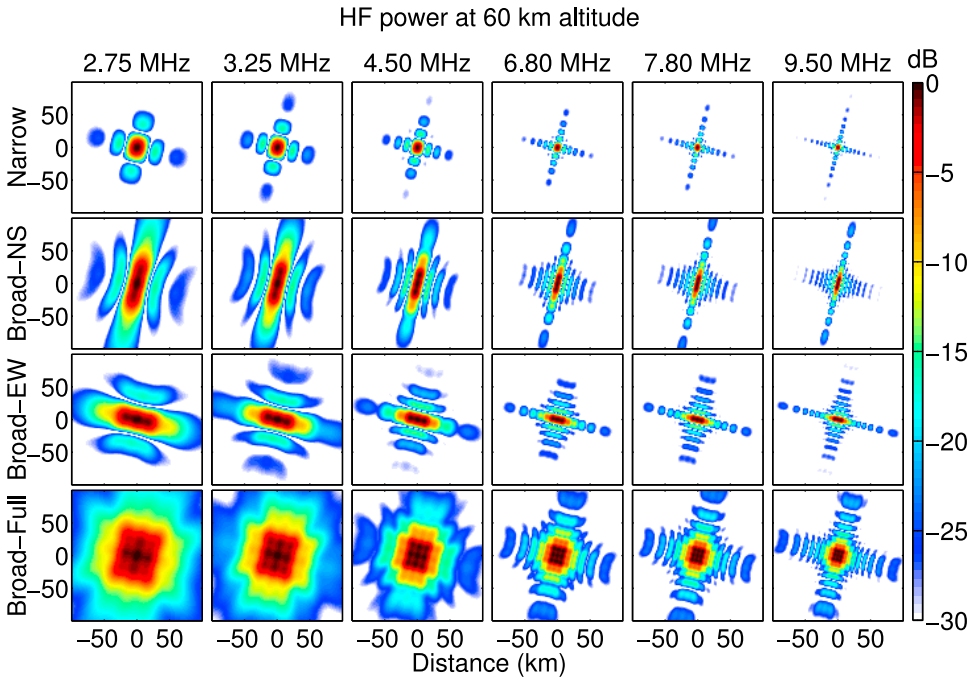

Figure 1. HF power pattern (relative to center of beam) into the ionosphere from HAARP beam modes.

detected with high signal-to-noise ratio, and demonstrate some features not visible at longer distances, like cavity resonance effects and elliptical polarizations resulting from multiple ionospheric reflections [*Stubbe et al.*, 1982].

[15] For proper comparison of the different HF frequencies and beam motions, we must have some knowledge of whether the natural generation conditions varied during the 28-minute period. Such a determination is difficult, in general, since even a combination of diagnostic instruments, such as a magnetometer and a riometer, cannot reliably assess generation conditions in the absence of a direct observation of the ELF generation strength [*Rietveld et al.*, 1987; *Jin et al.*, 2009, 2011].

[16] We implemented two strategies to mitigate uncertainty resulting from this inherent variability in generation conditions. First, the experiment was repeated many times so that general trends could be observed and so that what we can present a representative case. Second, the four-minute cycle for 3.25 MHz is transmitted twice, at the beginning and end, to allow some assessment of whether generation conditions have changed substantially over the 28-minute period. Experimental cases with overly unstable generation conditions, either a rapidly changing magnetometer value, or a large difference between the 3.25 MHz at the beginning and end, were discounted. The remaining cases still contain some smaller and slower change in generation conditions over the 28-minute period, but the repetition of the 3.25 MHz cycle allows the first derivative of these changes to be effectively calculated so that all the ELF amplitudes can be scaled according to their position within the 28-minute period.

[17] Figure 3 shows an example of the result from one representative case. Each panel show the amplitude received at Chistochina in the vertical axis, and the transmitted ELF/VLF frequency in the horizontal axis. The rows correspond to the four beam spacing modes while the columns represent the six HF frequencies. The panels are labeled with the minute within the 28-minute sequence that each was transmitted. Error bars are shown based on the noise levels at the time of the experiment, which was approximately 0.012 pT for a 2-second coherent integration and roughly constant as a function of frequency. However, these error bars are quite small. Figure 2 is taken from this same experimental period. It can be seen in this case that the 3.25 MHz signal was roughly the same amplitude at the beginning and the end of the cycle, which provides some confidence that the generation conditions were stable overall.

[18] In all the plots, a common trend is visible, with the frequency response demonstrating peaks roughly at multiples of 2 kHz. This pattern (observable near to the generation region) is similar to previously presented frequency sweeps [e.g., *Stubbe et al.*, 1982; *Rietveld et al.*, 1989], and is due to resonances with the cavity between the Earth and

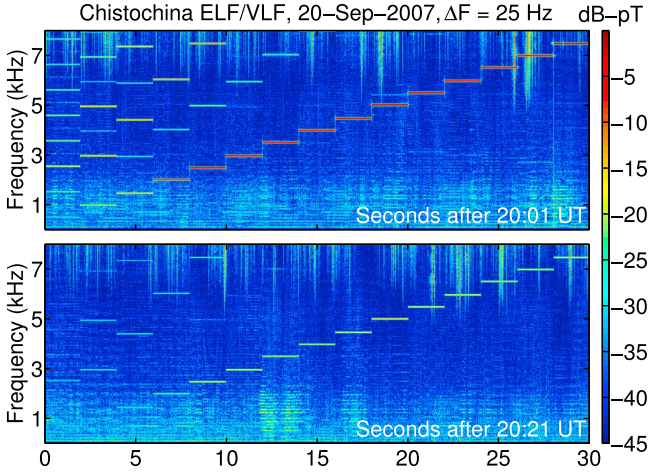

Figure 2. Spectrogram of HAARP-generated signals during HF beam diagnostic experiment, received at Chistochina.

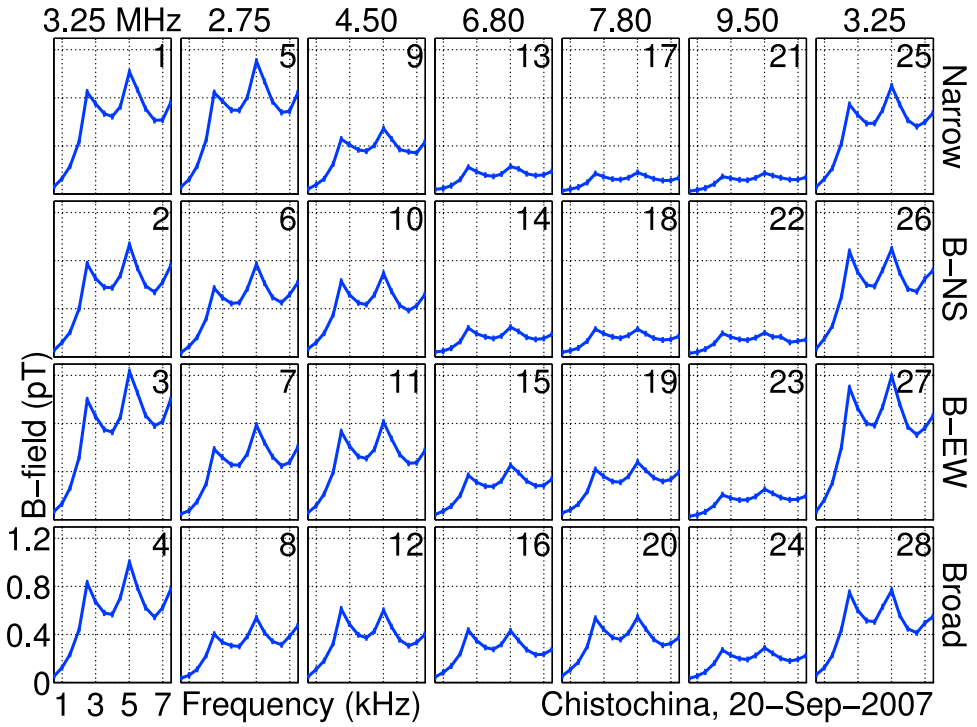

Figure 3. An example of the magnetic field amplitudes received at Chistochina as a function of minutes into the experiment (indicated in the top left corner of each panel) and frequency. The rows and columns of panels correspond to beam shape and HF frequency, respectively, over the 28 min of the experiment. The 3.25 MHz beam shapes are repeated at the end of the experiment. The experiment was conducted on 20-September-2007, 20:00–20:30 UT.

ionosphere. Note that 2 kHz is roughly the frequency where the reflection height is close to one half of a wavelength, or 75 km, so that the ionospherically reflected signal is in phase with the transmitted signal. In this particular example, the 4 kHz resonance was more intense than the 2 kHz resonance, although in many of the other repetitions of this experiment, the 2 khz resonance was stronger.

[19] To emphasize the variations between the formats, we normalize all received amplitudes by the amplitudes of the 3.25 MHz narrow beam, which provides a good basis for comparison (and normalization) for several reasons: (1) It produces strong ELF/VLF amplitudes, (2) it does not lose substantial radiated power when the beam is broadened, (3) it is a very common mode that has been used in past HAARP experiments, and (4) this beam mode is repeated twice in the 28-minute experiment.

[20] The ELF/VLF amplitudes are also normalized by the radiation efficiency HAARP (i.e., the fraction of the maximum 3.6 MW radiated power) to account for the reduced power levels for the broadened beam. The latter normalization is only approximately accurate, since the relationship between HF power and ELF amplitude is not precisely linear [*Barr and Stubbe*, 1991b; *Moore et al.*, 2006], but normalizing by HAARPs efficiency does help account for the loss of radiated power in the broad beam.

[21] The normalized results are shown in Figure 4. The panels with blue traces show each of the 24 combinations of beam modes and HF frequencies, as reflected by the labels in the top and left edges. The panels with gray lines, along the top and left, are the averages of the (pre-normalized, linear scale) signals for the different HF frequencies, and beam shapes, so that the effect of each parameter can be independently viewed. These row and column sums also appear in later figures. The error bars shown are larger because in taking the ratio of two numbers, the errors of both add up.

[22] There are some limitations to this experiment. Furthermore, the methods of adjusting for the electrojet strength and the HF radiated power are imperfect. As this experiment was repeated many times, we discuss here only those features that arise repetitively in the experiments, even though we show a single representative example. The effect of noise and interference (most prominently from distant lightning-generated impulses) are reflected in the error bars. Since the chosen frequencies do not occur near harmonics of 60 Hz power line frequency, it was not necessary to apply adaptive removal of power line interference, as in *Cohen et al.* [2010d].

[23] Generated amplitudes generally decrease with increasing HF frequency, with two exceptions: (1) The 2.75 MHz signal is weaker than 3.25 MHz for the broader beams. This may be due to the fact that HAARP is radiating substantially less power, and the amplitude does not necessarily scale with power [*Moore et al.*, 2006], so correcting proportional to the radiated power is imperfect. (2) The 7.8 MHz signal is slightly stronger than the 6.8 MHz. However, examination of other repetitions of the same experiment shows that this 7.8 MHz increase is not a common feature. It is more likely that in

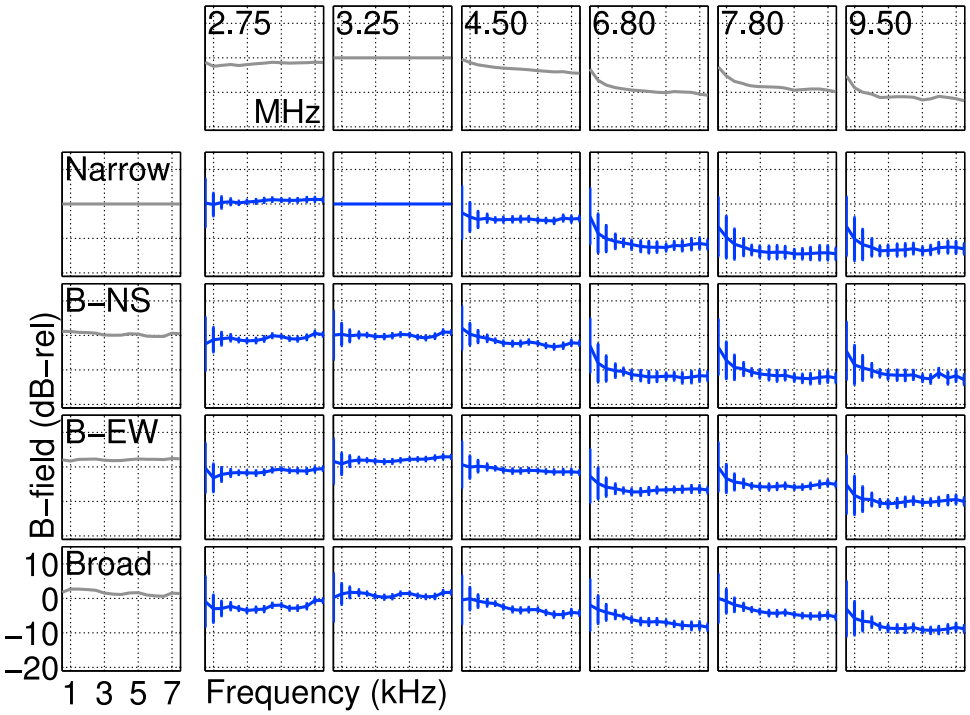

Figure 4. The results from Figure 3 after adjusting for electrojet changes and HF radiated power. The panels with gray traces show averages for the respective rows and columns.

this particular experimental run, the generation conditions briefly strengthened during the 7.8 MHz minutes, which is not removed by the aforementioned electrojet correction technique.

[24] It should be noted that the ERP is fundamentally coupled to the HF frequency with HAARP, since higher HF frequencies create tighter beam in the near-field coupled HF array, so comparing the 3.25 MHz narrow beam with 9.50 MHz is not a strict comparison of the comparative generation of those HF frequencies, because generated amplitudes are also a function of ERP [*Barr and Stubbe*, 1991b; *Moore et al.*, 2006]. However, the 9.50 MHz broad beam spreads out the HF energy over an area roughly the same area as the 3.25 MHz narrow beam, yet the generated ELF/VLF amplitudes are still 5–10 dB weaker, implying that increasing HF frequency does results in less ELF/VLF generation. This result is consistent with past findings [*James*, 1985; *Barr and Stubbe*, 1991a; *Taranenko et al.*, 1992] and is due to the fact that higher HF frequencies encounter less absorption from ionospheric collisions and therefore heat less effectively.

[25] Furthermore, beam broadening appears to have a noticeable effect on the data. Overall, as seen in the gray panels on the left, broadening raises the signal amplitude by 0–4 dB. For the Broad-EW and fully broad beams, this effect decreases with higher ELF frequencies, whereas with Broad-EW, the amplitude increase is closer to uniform as a function of ELF frequency.

[26] In addition, for the higher HF frequencies there appears to be a noticeable decrease in amplitude with increasing ELF frequency up to ~3 kHz. Another way to view this is that the generation at lower ELF frequencies is less dependent on HF frequency. However, this trend is not clearly distinguishable above the noise floor, and does not show up in the theoretical model discussed later, and may thus not be physical.

4. Theoretical Model

[27] The observed signals can be predicted utilizing a pair of theoretical models which predicts the ELF/VLF radiation both on the ground and in the ionosphere, as described by *Cohen et al.* [2010b, 2010a] and briefly reviewed here. An HF heating model (similar to that by *Tomko* [1981] and *Rodriguez* [1994]) is used to derive a set of current sources, which then lead to ELF/VLF fields on the ground and through the ionosphere with a full-wave propagation code.

[28] In the HF heating model, the ionosphere is divided into a 3D grid, and the HF power propagates upward through that grid. The HF heating simulation evolves forward in discrete time steps. A realistic pattern of HAARP HF radiation, including sidelobes, is used as input to the bottom of the ionosphere. At each altitude, both the bending of the HF wave, and the absorption of the wave from collisions, are calculated, and the absorbed power is used to evolve the electron temperature (at each grid point)via an energy balance equation that accounts for the absorbed HF energy, and the energy lost by electrons to neutrals from elastic and inelastic collisions. The use of this energy balance equation assumes that the electron temperature distribution remains Maxwellian, an assumption which is only approximately true.

[29] The resulting electron temperature is used to calculate the collision frequency, and ionospheric conductivities. The collision frequency is used as input into the next time step, since the absorption of subsequent HF energy is dependent on HF energy absorbed previously, resulting in an effect known

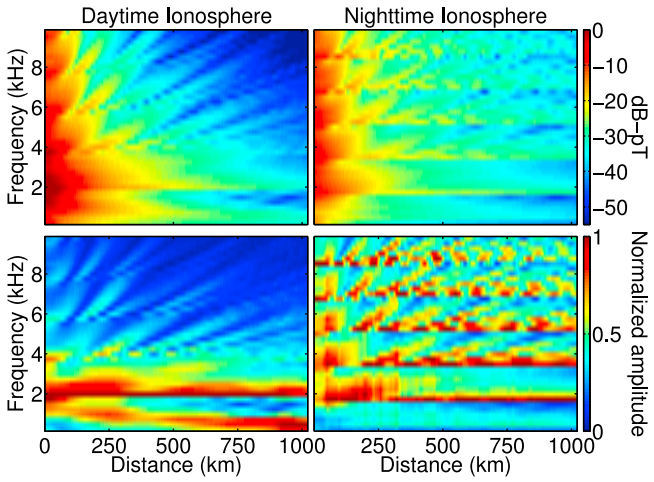

Figure 5. Calculated variation of frequency response by distance. (top) The absolute magnetic field amplitude, calculated from the model. (bottom) The same calculations, after each column (distance) is normalized by the peak amplitude at that distance, to show the character of the frequency response. Left and right columns are with two different ionospheric profiles for daytime and nighttime conditions.

as 'self-absorption'. The remaining HF power propagates upward to the next altitude. Over the course of several ELF/VLF cycles, the ionospheric conductivity reaches a sinusoidal steady state at each grid point, and the first harmonic of this steady state curve is extracted, separately for the Hall and Pedersen conductivities. The Parallel conductivity changes are ignored since it is assumed that the high conductivity in the direction of the magnetic field will act to rapidly cancel out any modulated currents in that direction.

[30] At each grid point, the extracted conductivity amplitudes and phases yield a current source when multiplied with an assumed electrojet field strength (taken here to be 10 mV/m, directed to geomagnetic north). The resulting currents are input into a numerical model of ELF/VLF wave propagation described by *Lehtinen and Inan* [2008, 2009]. The model calculates a Fourier-decomposed solution which avoids the numerical swamping that often plagues ELF/VLF propagation models. On the other hand, the model is much more computationally efficient compared to finite difference methods. The model predicts the electric and magnetic fields at all locations within, below, and above the ionosphere. The ionosphere is assumed to be time invariant and horizontally stratified, which is not true for the case of HAARP heating since the collision frequency above HAARP is affected by the heating. Nevertheless, *Lehtinen and Inan* [2008] find that this error is likely no more than 20–30%. The propagation model also assumes a flat Earth. For a source at 80 km on a curved surface, the distance along the Earth that obscures that source below the horizon is ~1000 km, so the model is considered valid out to about this distance.

[31] Both models assume an ionospheric electron density profile typical for high latitude winter conditions (either daytime of nighttime), taken from the International Reference Ionosphere, with exponential decrease in electron density below the bottom boundary of the model. The electron density is assumed to remain constant during the heating, ignoring much slower chemical effects of the heating that may change the electron density profile [*Milikh and Papadopoulos*, 2007]. The geomagnetic field orientation used is realistic and is taken from the IGRF-10 model assuming nighttime conditions. The electrojet is taken to arise from an electric field pointed geomagnetically to the north, with magnitude 10 mV/m.

[32] Figure 5 shows the results calculated at a series of ELF/VLF frequencies. The top two panels shows the predicted horizontal magnetic fields as a function of distance from the HF array, for both daytime (left) and nighttime (right) ionospheres. Although the model used is fully 3D, and uses both a nonvertical magnetic field and an asymmetric and realistic HAARP HF input, the fields as a function of distance are calculated by taking an average of the fields around a circle centered at each distance, so that what is shown is an azimuthal average of the magnetic field as a function of distance. At nearby distances (<100 km) the ~2 kHz cavity resonance peaks can be easily observed, and this feature fades away at a distance of ~250 km, for both daytime and nighttime ionosphere. For the daytime model, the 2 kHz resonance is strongest at all distances, however for the nighttime model, the 4 khz and sometimes even 6 kHz and 8 kHz peaks can be as strong or stronger than the 2 kHz peak. This is likely due to the high reflectivity of the ionosphere at nighttime, which leads to a more efficient cavity resonator effect. Some earlier studies *Kuo et al.* [2008] have suggested that peaks at higher order resonances, ~8 kHz, may be due to the interaction of generated VLF waves with ionospheric irregularities. However, the model here assumes a smooth ionosphere, so our results indicate that for nighttime experiments, resonance peaks at 4, 6, or 8 kHz may be possible even without ionospheric density irregularities.

[33] Beyond this distance, the defining feature is the interference pattern of multiple waveguide modes, which can be seen as streaks which move upward in frequency with increasing distance. This pattern is similar in nature to the V-shaped streaks of an interference pattern observed by satellites in flying over a thunderstorm [*Parrot et al.*, 2008]. The entire radiation pattern attenuates faster with distance for the daytime ionosphere than for the nighttime ionosphere.

[34] The lower plots of Figure 5 show the frequency response normalized at each distance to the peak amplitude, and plotted on a linear scale. These plots therefore reveal the changing frequency response as a function of distance. For the daytime ionosphere, the 2 kHz and 4 kHz spectral peaks are most intense, and even out to 1000 km distance, the 2 kHz spectral peak is very well defined. On the other hand, the spectral peaks closer to 8 kHz are even stronger, due to more efficient reflection off the ionosphere at those frequencies. Also, all of the spectral peaks linger to some extent out to 1000 km.

[35] We now apply the model to explain and compare to the measurements made at Chistochina. We note first that an exact and absolute comparison between theory and data is made complicated by a number of factors, including the experimental limitations mentioned earlier, as well as the uncertainty in selecting the ionospheric profile for the model, and the small-scale features (10s of km) that may be present in the radiation pattern on the ground.

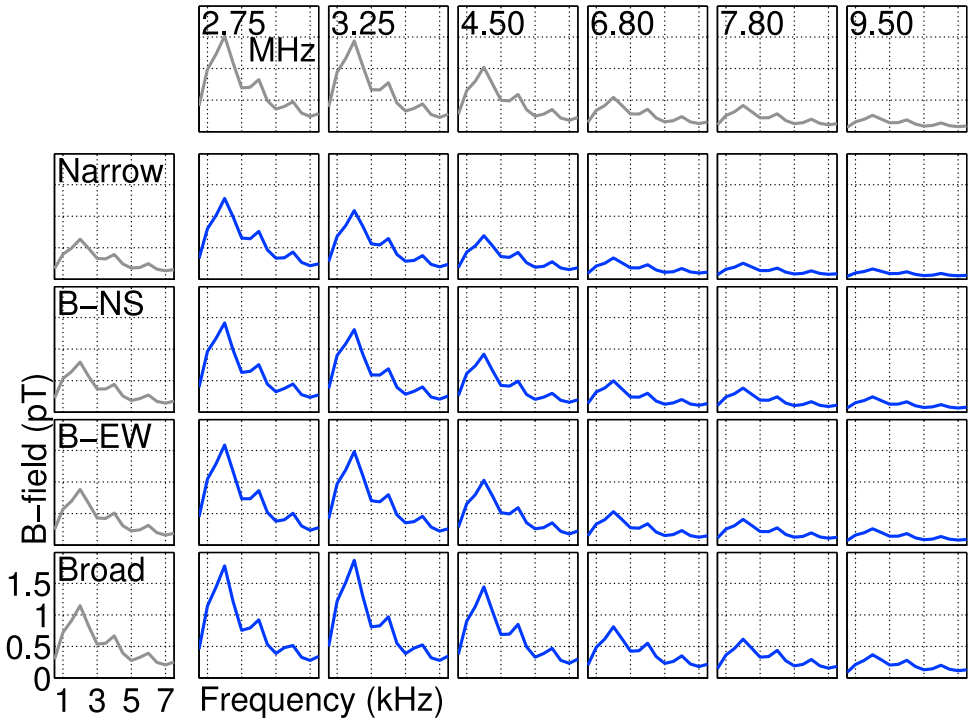

Figure 6. Calculations of the varying magnetic field received at Chistochina. The panels with gray traces show averages for the respective rows and columns. These calculations can be directly compare to data in Figure 3.

[36] Figure 6 shows the calculated ELF/VLF fields received at Chistochina. The results can be directly compared to those in Figure 3. The most important features are reproduced in the theoretical model, like the spectral peaks at multiples of 2–3 kHz, the decreasing generation amplitude with increasing HF frequency, and the increasing amplitude as the HF beam is broadened. In the theoretical model, the spectral peak that was measured at ~5 kHz actually appears at 4 kHz, and this difference is likely due to the fact that the ionospheric electron density profile is highly variable in the lower ionosphere, and not known precisely. The fact that the measured spectral peak is at a slightly higher frequency probably means that the reflection height is higher than in the model, which means that a lower electron density was present than that taken from the IRI.

[37] Figure 7 shows the calculated ELF/VLF fields received at Chistochina, normalized to 3.25 MHz and a narrow beam. The results can be directly compared to those in Figure 4. The effect of beam broadening is slightly larger in the theoretical model (0–6 dB instead of 0–4 dB). The effect of increasing HF frequency is roughly the same in the model as compared to the data (8–12 at 9.5 MHz). However, one feature captured in the model but not present in the data is that at high ELF frequencies, the effect of increasing the HF frequency is less pronounced. For instance, at 500 Hz modulation of 9.5 MHz, the signal strength is ~19 dB lower than the 3.25 MHz vertical beam. But at 7 kHz, this deficit is only ~5 dB. We do not have an explanation for this discrepancy, except for the possible frequency-dependent effects of noise in the data, or the uncertainty in the ionospheric profile in the model.

[38] Nonetheless, the reproduction of the most important features provides some validation of the theoretical model for the purpose of capturing the variation of beam parameters for these ELF/VLF frequency ranges. Having established the viability of the model for nearby measurements, we now present the predicted ELF/VLF wave amplitudes at further distances.

[39] We present the calculated amplitudes at two long distance sites (Kodiak, Juneau, ~700 km from HAARP) and the maximum amplitude injected to 700 km altitude (i.e., into the magnetosphere). The fields in all locations show the same dependence on HF frequency and beam width as was observed and modeled for short distances. However, some additional features are present.

[40] Figure 8 shows the calculated amplitudes received at Kodiak, 700 km away from HAARP to the southwest (i.e., close to geomagnetically south from HAARP). At Kodiak, the spectral peaks at 2 kHz multiples are substantially weaker if present at all, as the signal is now dominated by propagating waveguide modes rather than cavity resonances. There is a strong spectral peak above the first-order waveguide cutoff (which is 1.8 kHz), as high as 3 kHz.

[41] Figure 9 shows the calculated magnetic fields at Juneau, which is at a similar distance to Kodiak but in the southeast direction (i.e., close to geomagnetically east from HAARP). At Juneau, the same 2–3 kHz spectral peak appears, but the signals below 1kHz are reasonably strong, as well. Overall, however, the signals are a factor of ~2 weaker than they are at Kodiak. These results are both consistent with the observational results of *Cohen et al.* [2008a], who observed an azimuthal dependence to the frequency content, amplitude, and polarization, of the radiated signal from HAARP, identical to the Kodiak/Juneau differences theoretically shown here.

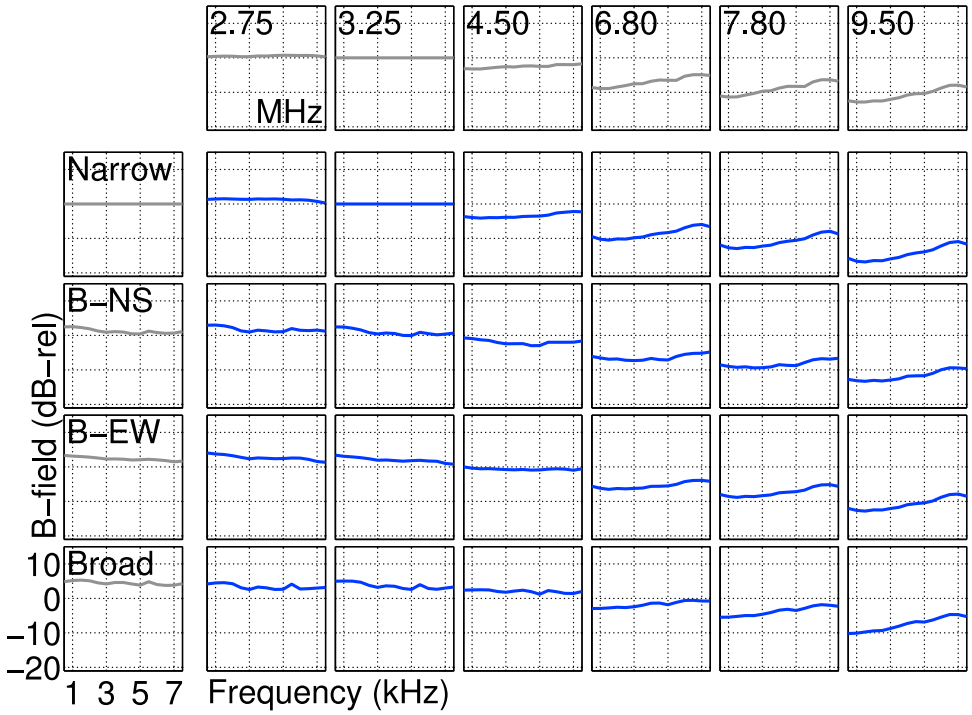

Figure 7. Calculations of the varying magnetic field received at Chistochina, after adjusting for HF power, and normalizing to 3.25 MHz, similarly to Figure 4. The panels with gray traces show averages for the respective rows and columns. These calculations can be directly compare to data in Figure 4.

[42] Finally, we present the theoretical predictions for the power radiated upward into the magnetosphere, using a method outlined and utilized in *Cohen et al.* [2011]. The upward Poynting flux is integrated over a horizontal slice at 700 km altitude, corresponding roughly to the altitude where the DEMETER satellite flew over HAARP [*Piddyachiy et al.*, 2008] to detect ELF/VLF radiated signals (Figure 10).

[43] The radiation emitted into the magnetosphere is not necessarily proportional to the radiation emitted into the Earth-ionosphere waveguide, most importantly because differences

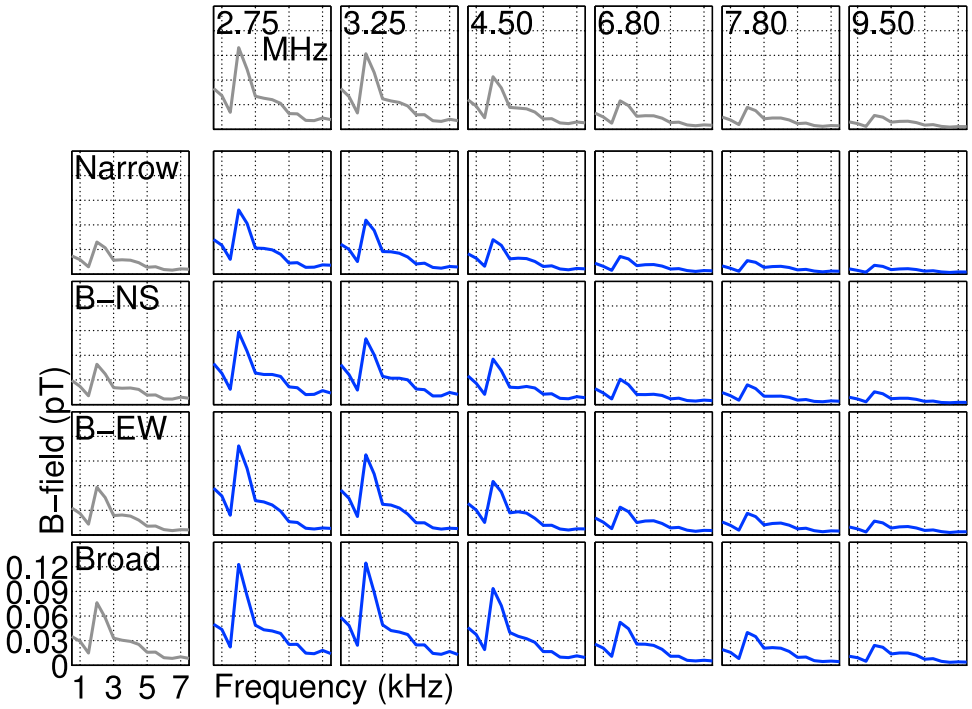

Figure 8. The same theoretical calculations as in Figure 6, but for the Kodiak receiver site.

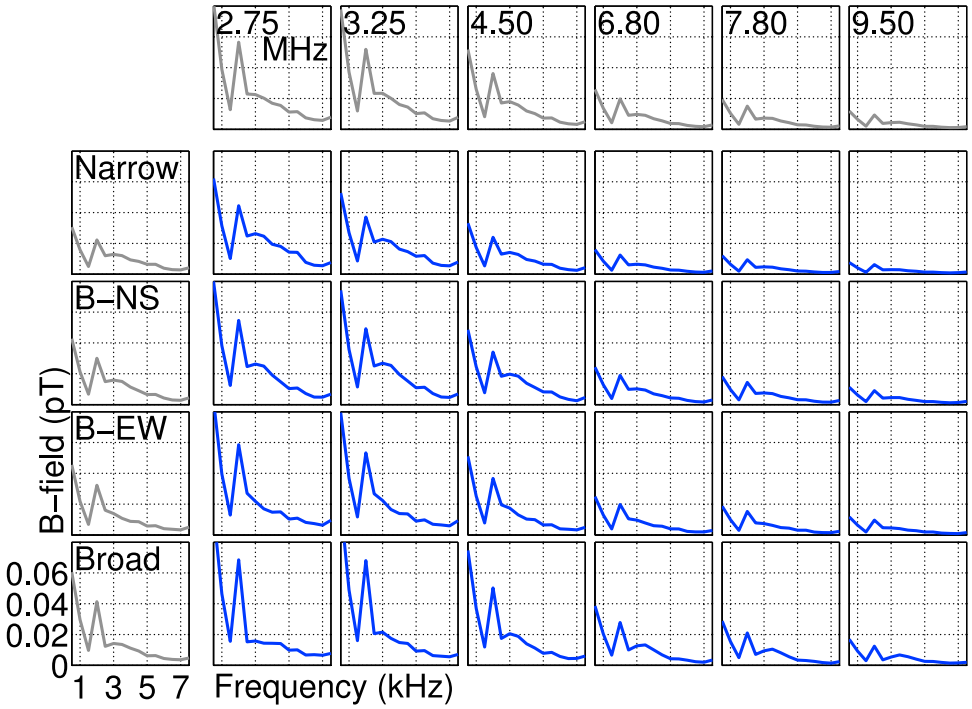

Figure 9. The same theoretical calculations as in Figure 6, but for the Juneau receiver site.

in the ionospheric electron density profile affect ratio of upward power to downward power. However, for the purposes of assessing the role of HF beam parameters (ERP and HF frequency), both the ground and magnetospheric signals react similarly for ELF/VLF generation above 1 kHz.

[44] Below 1 kHz, however, there are some important differences. Consistent with the results of *Cohen et al.* [2011], who calculated the frequency response for 3.25 MHz narrow beam, the power injected into the magnetosphere rises to a peak near 1 kHz of ~1 W, and then falls monotonically with increasing frequency. In *Cohen et al.* [2011], the peak at 1 kHz predicted in the magnetosphere was attributed to decreasing conductivity modulation above 1 kHz, and decreasing propagation and radiation efficiency below 1 kHz.

[45] However, as the HF frequency increases, the peak at 1 kHz actually decreases, and then vanishes. This result

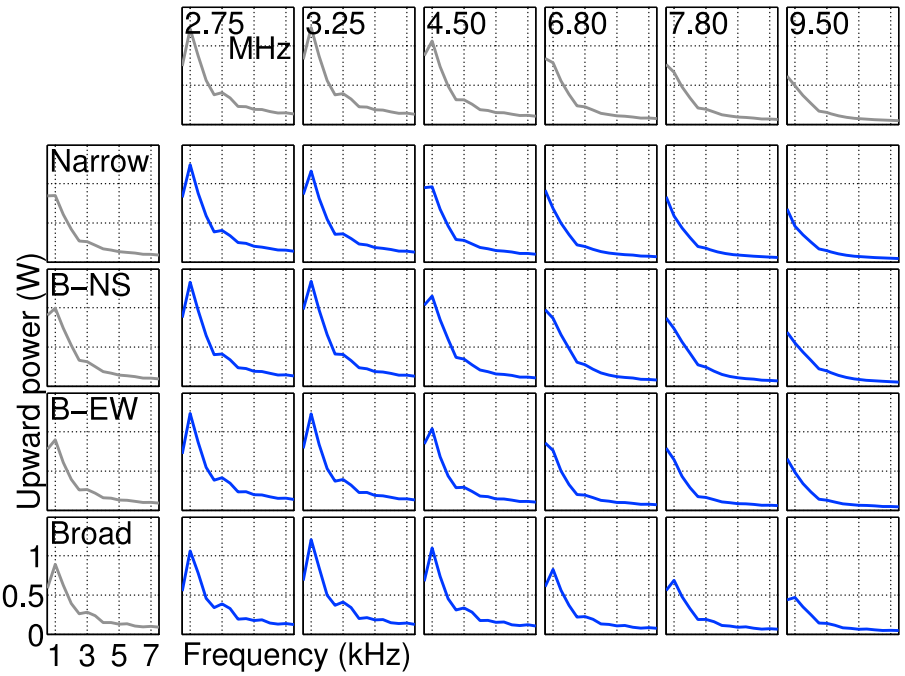

Figure 10. The same theoretical calculations as in Figure 6, but calculated at 700 km altitude.

could be due to the fact that at higher HF frequencies, the absorption and consequent ELF/VLF generation occurs at slightly higher altitudes. In addition, the 1 kHz peak also becomes more pronounced as the beam is broadened, since the broadening decreases the ERP and therefore lowers the altitude of generation [*Cohen*, 2010, p.49]. With less ionosphere between the source and the top of the magnetosphere, the decrease in radiation efficiency becomes slightly less important.

[46] **Acknowledgments.** This work has been supported by ONR award N0014-09-1-0100 and AFRL award FA9453-11-C-0011 to Stanford University. IGRF model calculations taken from http://omniweb.gsfc.nasa.gov/vitmo/cgm_vitmo.html. IRI model calculations taken from http://omniweb.gsfc.nasa.gov/vitmo/iri_vitmo.html.

[47] Robert Lysak thanks the reviewers for their assistance in evaluating this paper.

References

Barr, R., and P. Stubbe (1991a), ELF radiation from the Tromsø "super heater" facility, *Geophys. Res. Lett.*, *18*(6), 1035–1038.

Barr, R., and P. Stubbe (1991b), On the ELF generation efficiency of the Tromsø "super heater" facility, *Geophys. Res. Lett.*, *18*(11), 1971–1974.

Barr, R., P. Stubbe, M. T. Rietveld, and H. Kopka (1986), ELF and VLF signals radiated by the 'polar electrojet antenna': Experimental results, *J. Geophys. Res.*, *91*(A4), 4451–4459.

Barr, R., P. Stubbe, and H. Kopka (1991), Long-range detection of VLF radiation produced by heating the auroral electrojet, *Radio Sci.*, *24*(4), 871–879.

Cohen, M. B. (2010), ELF/VLF phased array generation via frequency-matched steering of a continuous HF ionospheric heating beam, PhD thesis, Stanford Univ., Stanford, Calif.

Cohen, M. B., M. Gołkowski, and U. S. Inan (2008a), Orientation of the HAARP ELF ionospheric dipole and the auroral electrojet, *Geophys. Res. Lett.*, *35*, L02806, doi:10.1029/2007GL032424.

Cohen, M. B., U. S. Inan, and M. Gołkowski (2008b), Geometric modulation: A more effective method of steerable ELF/VLF wave generation with continuous HF heating of the lower ionosphere, *Geophys. Res. Lett.*, *35*, L12101, doi:10.1029/2008GL034061.

Cohen, M. B., U. S. Inan, M. Gołkowski, and N. G. Lehtinen (2010a), On the generation of ELF/VLF waves for long-distance propagation via steerable HF heating of the lower ionosphere, *J. Geophys. Res.*, *115*, A07322, doi:10.1029/2009JA015170.

Cohen, M. B., U. S. Inan, M. Gołkowski, and M. J. McCarrick (2010b), ELF/VLF wave generation via ionospheric HF heating: Experimental comparison of amplitude modulation, beam painting, and geometric modulation, *J. Geophys. Res.*, *115*, A02302, doi:10.1029/2009JA014410.

Cohen, M. B., U. S. Inan, and E. P. Paschal (2010c), Sensitive broadband ELF/VLF radio reception with the AWESOME instrument, *IEEE Trans. Geosci. Remote Sens.*, *48*(1), 3–17, doi:10.1109/TGRS.2009.2028334.

Cohen, M. B., R. K. Said, and U. S. Inan (2010d), Mitigation of 50/60 Hz power-line interference in geophysical data, *Radio Sci.*, *45*, RS6002, doi:10.1029/2010RS004420.

Cohen, M. B., U. S. Inan, D. Piddyachiy, N. G. Lehtinen, and M. Golkowski (2011), Magnetospheric injection of ELF/VLF waves with steerable HF heating of the lower ionosphere, *J. Geophys. Res.*, *116*, A06308, doi:10.1029/2010JA016194.

Ferraro, A. J., H. S. Lee, R. Allshouse, K. Carroll, A. A. Tomko, F. J. Kelly, and R. G. Joiner (1982), VLF/ELF radiation from the ionospheric dynamo current system, modulated by powerful HF signals, *J. Atmos. Terr. Phys.*, *44*(12), 1113–1122.

Getmantsev, C. G., N. A. Zuikov, D. S. Kotik, N. A. Mironenko, V. O. Mityakov, Y. A. Rapoport, V. Y. Sazanov, V. Y. Trakhtengerts, and V. Y. Eidman (1974), Combination frequencies in the interaction between high-power short-wave radiation and ionsopheric plasma, *J. Exp. Theor. Phys.*, *20*, 101–102.

Gołkowski, M., U. S. Inan, A. R. Gibby, and M. B. Cohen (2008), Magnetospheric amplification and emission triggering by ELF/VLF waves injected by the 3.6 MW HAARP ionospheric heater, *J. Geophys. Res.*, *113*, A10201, doi:10.1029/2008JA013157.

Golkowski, M., M. B. Cohen, D. L. Carpenter, and U. S. Inan (2011), On the occurrence of ground observations of ELF/VLF magnetospheric amplification induced by the HAARP facility, *J. Geophys. Res.*, *116*, A04208, doi:10.1029/2010JA016261.

Inan, U. S., et al. (2004), Multi-hop whistler-mode ELF/VLF signals and triggered emissions excited by the HAARP HF heater, *Geophys. Res. Lett.*, *31*, L24805, doi:10.1029/2004GL021647.

James, H. (1985), The ELF spectrum of artificially modulated D/E-region conductivity, *J. Atmos. Terr. Phys.*, *47*(11), 1129–1142.

Jin, G., M. Spasojevic, and U. S. Inan (2009), Relationship between electrojet current strength and ELF signal intensity in modulated heating experiments, *J. Geophys. Res.*, *114*, A08301, doi:10.1029/2009JA014122.

Jin, G., M. Spasojevic, M. B. Cohen, U. S. Inan, and N. G. Lehtinen (2011), The relationship between geophysical conditions and elf amplitude in modulated heating experiments at haarp: Modeling and experimental results, *J. Geophys. Res.*, *116*, A07310, doi:10.1029/2011JA016664.

Kuo, S. P., Y.-L. Wu, R. Pradipta, J. A. Cohen, and M. C. Lee (2008), Vlf wave generation by amplitude-modulated hf heater waves at Gakona, Alaska, *Geophys. Res. Lett.*, *35*, L13101, doi:10.1029/2008GL034414.

Lehtinen, N. G., and U. S. Inan (2008), Radiation of ELF/VLF waves by harmonically varying currents into a stratified ionosphere with application to radiation by a modulated electrojet, *J. Geophys. Res.*, *113*, A06301, doi:10.1029/2007JA012911.

Lehtinen, N. G., and U. S. Inan (2009), Full-wave modeling of transionospheric propagation of VLF waves, *Geophys. Res. Lett.*, *36*, L03104, doi:10.1029/2008GL036535.

Lunnen, R. J., H. S. Lee, A. J. Ferraro, T. W. Collins, and R. F. Woodman (1984), Detection of radiation from a heated and modulated equatorial electrojet current system, *Nature*, *311*(13), 134–135.

McCarrick, M. J., D. D. Sentman, A. Y. Wong, R. F. Wuerker, and B. Chouinard (1990), Excitation of ELF waves in the schumann resonance range by modulated HF heating of the polar electrojet, *Radio Sci.*, *25*(6), 1291–1298.

Milikh, G. M., and K. Papadopoulos (2007), Enhanced ionospheric ELF/VLF generation efficiency by multiple timescale modulated heating, *Geophys. Res. Lett.*, *34*, L20804, doi:10.1029/2007GL031518.

Moore, R. C., U. S. Inan, and T. F. Bell (2006), Observations of amplitude saturation in ELF/VLF wave generation by modulated HF heating of the auroral electrojet, *Geophys. Res. Lett.*, *33*, L12106, doi:10.1029/2006GL025934.

Moore, R. C., U. S. Inan, T. F. Bell, and E. J. Kennedy (2007), ELF waves generated by modulated HF heating of the auroral electrojet and observed at a ground distance of ∼4400 km, *J. Geophys. Res.*, *112*, A05309, doi:10.1029/2006JA012063.

Parrot, M., U. S. Inan, and N. G. Lehtinen (2008), V-shaped VLF streaks recorded on DEMETER above powerful thunderstorms, *J. Geophys. Res.*, *113*, A10310, doi:10.1029/2008JA013336.

Piddyachiy, D., U. S. Inan, and T. F. Bell (2008), DEMETER observations of an intense upgoing column of ELF/VLF radiation excited by the HAARP HF, *J. Geophys. Res.*, *113*, A10308, doi:10.1029/2008JA013208.

Rietveld, M. T., H. P. Mauelshagen, P. Stubbe, H. Kopka, and E. Nielsen (1987), The characteristics of ionospheric heating-produced ELF/VLF waves over 32 hours, *J. Geophys. Res.*, *92*(A8), 8707–8722.

Rietveld, M. T., P. Stubbe, and H. Kopka (1989), On the frequency dependence of ELF/VLF waves produced by modulated ionospheric heating, *Radio Sci.*, *24*(3), 270–278.

Rodriguez, J. V. (1994), Modification of the Earth's ionosphere by very low frequency transmitters, PhD thesis, Stanford Univ., Stanford, Calif.

Stubbe, P., H. Kopka, and R. L. Dowden (1981), Generation of ELF and VLF waves by polar electrojet modulation: Experimental results, *J. Geophys. Res.*, *86*(A11), 9073–9078.

Stubbe, P. H., H. Kopka, M. T. Rietveld, and R. L. Dowden (1982), ELF and VLF generation by modulated heating of the current carrying ionosphere, *J. Atmos. Terr. Phys.*, *44*(12), 1123–1135.

Taranenko, Y. N., U. S. Inan, and T. F. Bell (1992), VLF-HF heating of the lower ionosphere and ELF wave generation, *Geophys. Res. Lett.*, *19*(1), 61–64.

Tomko, A. A. (1981), Nonlinear phenomena arising from radio wave heating of the lower ionosphere, PhD thesis, Penn. State Univ., State College.

Villaseñor, J., A. Y. Wong, B. Song, J. Pau, M. McCarrick, and D. Sentman (1996), Comparison of ELF/VLF generation modes in the ionosphere by the HIPAS heater array, *Radio Sci.*, *31*(1), 211–226.